Journal of Magnetic Resonance **141,** 261–270 (1999)
Article ID jmre.1999.1884, available online at http://www.idealibrary.com on IDEAL®

J Pulses for Multiplet-Selective NMR

M. Robin Bendall and Thomas E. Skinner*

*The Russell Grimwade School of Biochemistry and Molecular Biology, University of Melbourne, Parkville 3052, Victoria, Australia; and *Department of Physics, Wright State University, Dayton, Ohio 45435*

Received March 31, 1999; revised July 29, 1999

Exact product operator solutions have been obtained for the evolution of weakly coupled spin-$\frac{1}{2}$ I_mS_n systems during arbitrary RF irradiation of one spin. These solutions, which completely characterize the nature of *J*-coupling modulation during RF pulses, show that significant exchange occurs between single-spin magnetization and two-spin product operator states when the RF field strength is comparable to the coupling. In particular, a long ($t_p = [\sqrt{2}J]^{-1}$ s), low-power ($B_1 = J/2$ Hz), constant amplitude pulse applied on resonance to one spin in an IS system completely interconverts the spinstates $S_z \leftrightarrow 2S_xI_z$ and $S_x \leftrightarrow 2S_zI_z$ when the RF is applied to the S spins, and interconverts $S_x \leftrightarrow 2S_yI_y$ in 100% yield when the RF is applied to the I spins. Thus, these "*J* pulses," which select a bandwidth approximately equal to *J* Hz, may replace any combination of a $(2J)^{-1}$ delay period and a consecutive hard 90° pulse in any polarization transfer or multiple quantum sequence. Although these rectangular pulses are highly frequency selective, in general they increase the replaced $(2J)^{-1}$ period by only a modest 40%, a time saving of a factor of 5 compared to existing pulses exhibiting the same selectivity. In favorable cases, there is no increase in duration of a pulse sequence using a particular type of *J* pulse, the 90^J variety, which accomplishes the third spin state transformation listed above. *J* pulses will be advantageous for systems subject to rapid signal loss from relaxation and more generally for the enhanced operation of pulse sequences via the use of *J* modulation during RF irradiation.

INTRODUCTION

In order to gain insight into the mechanics of a vector model of spin state transformations during RF irradiation (*1, 2*), we have calculated the evolution of the orthogonal product operator states during application of arbitrary RF waveforms to one spin of a weakly coupled spin-$\frac{1}{2}$ I_mS_n system, under a complete set of standard initial conditions (*3, 4*). Previous general treatments have dealt exclusively with the observable signal from initial in-phase magnetization in an IS system subject to arbitrary RF (*5, 6*) or in an I_mS_n system subject to CW irradiation (*7*). Our more comprehensive quantum mechanical solutions yield analytical expressions for a constant RF pulse that describe the interconversion of the orthogonal spin states in time, beginning with an arbitrary spin state. Thus, the equations define the conditions necessary for 100% transformation between two spin states. One general application of these spin state transformations, introduced here, is in frequency-selective NMR.

Frequency-selective RF pulses may be used to simplify complex spectra by selecting a subset of resonances. In multidimensional NMR they may be used to reduce the bandwidth of one or more dimensions to increase resolution for the same total acquisition time. Alternatively, they can eliminate one dimension to allow increased resolution in the remaining dimensions for the same acquisition time or to reduce the total experimental time (*8*). In 1D applications, such as in *in vivo* NMR, the object is to select a reduced number of desired resonances from a complex overlapping array of signals. Frequency-selective NMR is of increasing potential worth with increasing molecular weight as an aid in discrimination between more numerous signals, but selective pulses are not commonly used at present because they are long and there is loss of S/N via relaxation for large molecules. The methods described here replace existing delays within pulse sequences with selective pulses and so do not greatly increase the time length of the sequence.

Frequency-selective pulses are normally classified as *semiselective* if they operate over part of the spectrum and transform all lines of a multiplet uniformly. In this case the effective field during the pulse is usually assumed to be much greater than the coupling constant J of any multiplet, or the effects of coupling are suppressed, so that J evolution can be ignored during the pulse. The class of *selective* pulses is generally restricted to the excitation or inversion of only one line of the multiplet and for these the RF amplitude $B_1 \ll J$.

In this article we introduce the general concept of the utilization of J modulation during an RF pulse to selectively and completely transform a weakly coupled IS spin system between single-spin magnetization and two-spin product operator states, or vice versa. In the applications we describe, B_1 is of the same order as the coupling constant, and although all lines of the multiplet are affected uniformly, the bandwidth of the pulse only just covers the entire multiplet. Thus, in terms of frequency, these RF pulses are on the border between *selective* and *semiselective* pulses, and they are also selective with respect to the initial and final spin states. In the conventional

1090-7807/99 $30.00

use of frequency-selective pulses, the effects of scalar coupling are suppressed by decoupling or spin-locking the unselected spins during selective 90° pulses, or by the refocusing that occurs naturally during selective inversion pulses. By taking advantage of *J*-coupled motion during the RF irradiation we show that any consecutive combination of a hard 90° pulse and a $(2J)^{-1}$ free precession period in any pulse sequence may be replaced by a single frequency-selective pulse, and we will refer to this new class of RF pulse as "*J* pulses." Thus, *J* pulses are not distinguished from other selective pulses by shape, but by the precise match of pulse time t_p and B_1 amplitude necessary to provide an exact transformation between two spin states that would conventionally require a combination of a pulse and delay period for the conversion.

Our initial project in this general area showed that adiabatic inversion pulses could take the place of all or part of $(2J)^{-1}$ delay periods in pulse sequences (*1*) and that a time-dependent reduced scalar coupling constant was operative during the pulse—this was the basis of the vector model. One illustration of the reduced *J* was that an off-resonance spin-lock pulse on ^{1}H nuclei could be used to match the coupled precession of ^{15}N spins in NH_2 groups (angular rate $= \pm J$ Hz normally) with that of NH groups (angular rate $= \pm J/2$ Hz normally) based on a difference in chemical shift for the two types of groups in proteins, so that an INEPT transfer step was close to optimum for both groups (*1*). We noted that this was a modern pulsed application of off-resonance CW decoupling (*7*), a popular method prior to FT NMR. In closely related work, the approximate linear relation between $^1J_{HC}$ and chemical shift in biomolecules (*9*) and organic molecules (*10*) has since been used to match coupled precession in chemically different groups utilizing the same principles with adiabatic inversion pulses. Most recently, in a detailed analysis of adiabatic decoupling (*2*) we found that calculations of the reduced coupling constant using the vector model, and exact quantum mechanical calculations, gave indistinguishable results for a single adiabatic inversion pulse. However, the concept of a reduced coupling constant, and all the methods introduced in Refs. (*1, 2, 9, 10*), comply with the condition that B_1 or the effective field $B_e \gg J$. Accordingly, there is not a close relationship between these studies and the on-resonance *J* pulses introduced here for which $B_1 \approx J$.

Another area that may seem related is that of spin-tickling (*7*), or the SPT (or SPI) techniques (*11*), in which one line of a doublet is selectively inverted. For these methods $B_1 \ll J$ and, in the approximation used, the effect of *J* modulation is ignored during the pulse, so again there is not a close relation with *J* pulses. Inevitably, these three areas must merge at intermediate values of B_1. We will show in a subsequent publication how the spin physics alters dramatically between these regimes.

In the next section an outline is provided of the spin state transformations that can be generally achieved in pulse sequences using *J* pulses. This is followed by examples of specific applications of rectangular *J* pulses for frequency-selective NMR that can be usefully and easily implemented now. Comparisons are made with equivalent multidimensional methods. In a third section, *J* pulses are shown to have advantages over conventional frequency-selective techniques in terms of reducing the time length of pulse sequences. In the concluding section several areas for further development are noted that could make *J* pulses widely competitive with existing methods.

POSSIBLE SPIN STATE CONVERSIONS USING *J* PULSES

One example of a *J* pulse has already been described by Brondeau and Canet (*12*). They showed that for an IS spin system, an on-resonance long low-power rectangular RF excitation pulse ($B_1 = J/2$ Hz; length $t_p = (\sqrt{2}J)^{-1}$ s; phase *x*) will transform initial S_z to $2S_xI_z$. In consequence this pulse can substitute for the initial pulse sequence elements, 90[S, *x*]–$(2J)^{-1}$, in INEPT, where 90[S, *x*] signifies a 90° pulse of *x* phase on the S spins. The mechanism of the pulse can be described as the classical rotation of the two S-spin magnetizations (coupled to I spins along $\pm z$) by 180° around two effective fields, $B_e^{\pm}$, tilted at 45° from the *xy* plane by the $\pm J/2$ coupling fields (*12*). The pulse was first implemented as a DANTE train (*13*) to provide the equivalent of continuous low power, but using a high-power source. Rapid RF power switching is now routine, so this aspect is no longer needed.

We have found no other examples of *J* pulses in the NMR literature, but there are several other selective spin state transformations that can be generated from a detailed analysis of our exact analytical equations, which include the effects of scalar coupling, for an RF excitation pulse (*4*). A subset of these equations has been derived previously by Bazzo and Boyd for the particular case of an IS spin system as a 6×6 matrix (Eq. [6] of Ref. (*14*)). The matrix describes the interconversion of the six possible orthogonal spin states, S_x, S_y, S_z, $2S_xI_z$, $2S_yI_z$, and $2S_zI_z$, but these authors did not find any of the 100% spin state transformations that are possible within the set. Simplification of the 6×6 matrix for on-resonance irradiation reveals four conversions that occur in 100% yield under the same conditions of RF power and pulse length given above. The term in row 4, column 3 of the 6×6 matrix corresponds to the $S_z \rightarrow 2S_xI_z$ transformation described above. Brondeau and Canet (*12*) did not consider the inverse $2S_xI_z \rightarrow S_z$ conversion, but this is governed by the term in row 3, column 4. Furthermore, new forward and reverse transformations, $S_x \leftrightarrow 2S_zI_z$, are given by the terms in row 6, column 1 and row 1, column 6, respectively, of the 6×6 matrix. As one part of a subsequent comprehensive paper that matches quantum mechanical equations with vector descriptions, we will show that the most general 6×6 matrix can be derived from calculating the classical rotation of the S-spin magnetizations around the two effective fields, $B_e^{\pm}$, defined by the resultant of the RF field and

the coupling (see Eq. [5] below). One detail is that all four of the above spin state transformations are 180° rotations. Since these rotations include the effect of *J* coupling, we will call the RF pulses that induce the rotations "180^J" pulses.

In addition, we have derived exact product operator solutions for the effect of scalar coupling during arbitrary RF pulses on the I spins after excitation of the S spins (*3, 4*). These new calculations show that the irradiation interconverts four orthogonal spin states, S_x, $2S_yI_x$, $2S_yI_y$, and $2S_yI_z$. Although the induced rotations are now nonclassical in the sense that they are not simple linear rotations around the effective fields, the system can still be described in terms of exact analytical equations so that the rotation of magnetization vectors can be followed straightforwardly, both by calculation and by measurement. In particular, on-resonance pulses of *x* phase do not produce any of the $2S_yI_x$ spin state and, when $B_1 = J/2$ Hz, CW irradiation produces an oscillation between S_x and $2S_yI_y$ with some transitory $2S_yI_z$. Recently we provided the equations for this on-resonance oscillation for any B_1 and showed that the phenomenon could be used to comprehensively and quickly characterize the I-spin channel using signals from the S-spin channel, yielding several methods for determining the homogeneity of the applied RF (*15*). Another outcome is that S_x can be converted entirely to $2S_yI_y$ with an on-resonance low-power rectangular RF pulse on the I spins ($B_1 = J/2$ Hz; length $t_P = (\sqrt{2}J)^{-1}$ s; phase *x*). Although these are the same conditions as for the 180^J[S] pulses just described, the detailed analysis of these equations in terms of magnetization vectors (to be published as above) shows that the vectors associated with the I spin states rotate 90° from the $\pm z$ axes to the $\pm y$ axes and remain antiparallel at all times. The axis of rotation is the B_1 field and the $\pm J/2$ coupling fields are manifested in a nonlinear rate of rotation of the I spins in the *yz* plane and a nonlinear rate of precession of the S spins in the *xy* plane. Since the rotation induced by the RF is 90°, we named the pulse "90^J" and used it in the new methods for characterizing the I-spin channel (which also provides an easy means of calibrating $B_1 = J/2$ Hz (*15*)—see Experimental).

In summary, the above analysis shows that there are at least three potentially useful *J* pulses:

$$180^J[\mathrm{S}, x] \text{ for } S_z \leftrightarrow 2S_xI_z, \quad [\mathrm{A}]$$

$$180^J[\mathrm{S}, x] \text{ for } S_x \leftrightarrow 2S_zI_z, \quad [\mathrm{B}]$$

and

$$90^J[\mathrm{I}, x] \text{ for } S_x \leftrightarrow 2S_yI_y. \quad [\mathrm{C}]$$

In pulse sequences, the I and S labels and the *x* and *y* phases may be swapped at will. Thus, in a standard INEPT (*16*) portion of a pulse sequence without refocusing pulses,

$$90[\mathrm{S}, x]\text{–}(2J)^{-1}\text{–}\{90[\mathrm{S}, y];\ 90[\mathrm{I}]\}\text{–}(2J)^{-1}\ldots, \quad [\mathrm{D}]$$

$$180^J[\mathrm{S}, x] \text{ for } S_z \rightarrow 2S_xI_z \text{ may replace } 90[\mathrm{S}, x]\text{–}(2J)^{-1}; \quad [\mathrm{E}]$$

$$180^J[\mathrm{S}, y] \text{ for } S_y \rightarrow 2S_zI_z \text{ may replace } (2J)^{-1}\text{–}90[\mathrm{S}, y]; \quad [\mathrm{F}]$$

$$90^J[\mathrm{I}, x] \text{ for } S_y \rightarrow 2S_xI_y \text{ may replace } (2J)^{-1}\text{–}90[\mathrm{I}]; \quad [\mathrm{G}]$$

$$180^J[\mathrm{I}, x] \text{ for } 2I_zS_z \rightarrow I_x \text{ may replace } 90[\mathrm{I}]\text{–}(2J)^{-1}; \quad [\mathrm{H}]$$

and

$$90^J[\mathrm{S}, y] \text{ for } 2I_yS_x \rightarrow I_x \text{ may replace } 90[\mathrm{S}, y]\text{–}(2J)^{-1}. \quad [\mathrm{J}]$$

Also, 180^J as in scheme [E] can be used for the initial hard 90° excitation pulse in multiple quantum sequences (e.g., four-pulse HMQC (*17*)), and a 90^J pulse can substitute for any of the subsequent hard 90° pulses. Furthermore, each transformation is frequency selective because the applied RF power is weak. Consequently, any combination of a $(2J)^{-1}$ free precession period and a consecutive hard 90° pulse, in any polarization transfer or multiple quantum pulse sequence, for an IS spin system, can be replaced by a frequency-selective 180^J or 90^J pulse.

The exact analytical equations for the yield in transformations [A] and [B] as a function of resonance offset, for rectangular 180^J pulses, may be obtained from the tables in Ref. (*4*) or from the four relevant terms (specified above) in the bottom-left to top-right diagonal of the 6×6 matrix in Eq. [6] of Ref. (*14*). The same expression applies in each case and coincides with that provided by Brondeau and Canet for $S_z \rightarrow 2S_xI_z$ (*12*). It may be written as

$$\sin 2\alpha^+ \sin^2[\theta^+/2] - \sin 2\alpha^- \sin^2[\theta^-/2], \quad [1]$$

where

$$\theta^{\pm} = 2\pi B_e^{\pm} t_P, \quad [2]$$

$$\sin \alpha^{\pm} = [\Delta H \pm (J/2)]/B_e^{\pm}, \quad [3]$$

$$\cos \alpha^{\pm} = B_1/B_e^{\pm}, \quad [4]$$

and

$$(B_e^{\pm})^2 = B_1^2 + [\Delta H \pm (J/2)]^2, \quad [5]$$

where $B_1 = J/2$ Hz and $t_P = (\sqrt{2}J)^{-1}$ s to provide the conditions for the 180^J pulse, and ΔH is the resonance offset in Hertz. The corresponding equation for transformation [C] using a rectangular 90^J pulse (*4*) is

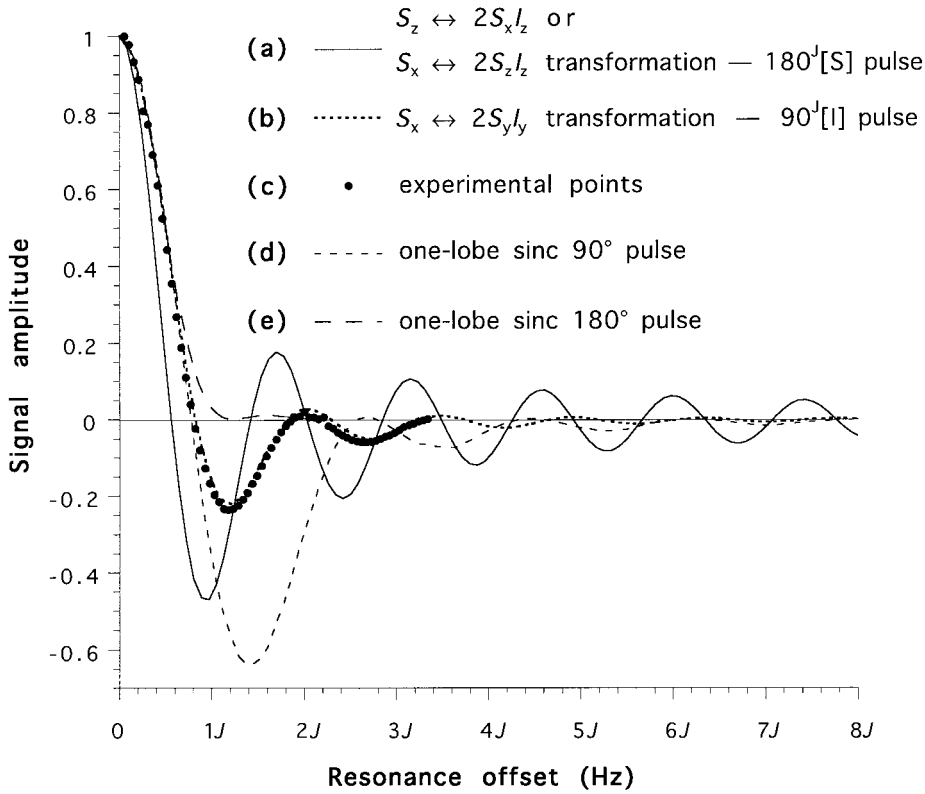

FIG. 1. Plots of signal magnitude versus resonance offset for (a) a rectangular 180^J pulse calculated using Eq. [1]; (b) a rectangular 90^J pulse calculated using Eq. [6]; (c) the 90^J pulse obtained by experimental measurement using sequence [M]; (d) a one-lobe sinc 90° pulse; and (e) a one-lobe sinc 180° pulse calculated using the Bloch equation. The Bloch equation excludes the effect of scalar coupling during the RF pulse. For the sinc-180 inversion pulse the extent of inversion between -1.0 and 1.0 units of S_z magnetization has been rescaled to vary between a signal magnitude of 1.0 and 0, respectively, for direct comparison with (a) to (d). (d and e) See Comparison with Conventional Pulses.

$$\sin[\alpha^+ - \alpha^-](\cos 0.5[\theta^+ - \theta^-] - \cos 0.5[\theta^+ + \theta^-]), \quad [6]$$

where the symbols have the same meanings as for Eq. [1].

The selectivity profiles given by Eqs. [1] and [6] are plotted in Figs. 1a and 1b, respectively, and the new Eq. [6] is confirmed by experiment in Fig. 1c as described under Experimental. The profiles demonstrate that the bandwidths of these J pulses are of the order of the J coupling constant. Since the length of the J pulses is $(\sqrt{2}J)^{-1}$ s, the replaced $(2J)^{-1}$ period is increased by only 40%, or $0.2J^{-1}$ s. The bandwidth of conventional selective RF pulses is approximately equal to or greater than the reciprocal of their length, i.e., $t_p \geq J^{-1}$ s for a bandwidth of J Hz. So, in comparison to conventional methods, a time saving of about a factor of 5 or more is achieved by substituting a J pulse for a $(2J)^{-1}$ precession period (this comparison is discussed in more detail in a later section). The advantage over conventional selective RF pulses will be important for application to large macromolecules and other systems subject to rapid signal loss from relaxation.

SPECIFIC APPLICATIONS OF RECTANGULAR J PULSES

From Fig. 1, the selectivity profile for the 90^J pulse is much better than that for 180^J in that the "sinc-like" oscillations are more rapidly damped with resonance offset for 90^J. Indeed, as discussed below, the profile for a 90^J rectangular pulse is competitive with that of conventional shaped pulses. Conversely, the rectangular 180^J profile is not competitive, although we suggest that it will be possible to shape 180^J pulses to improve their profiles.

A further advantage for 90^J in more complex pulse sequences is obtained by nesting this type of J pulse entirely within a free-precession period to avoid any increase in the time length of the sequence. For example, in triple-resonance methods, it is common to refocus the antiphase state of spin S relative to spin P and create the antiphase state with respect to spin I at the same time. Since the overall length of the free-precession period is determined by the smallest coupling constant, a 90^J pulse corresponding to the largest coupling constant can be inserted with no increase in the overall delay period.

This principle, as well as the selectivity of *J* pulses, is illustrated by the results in Figs. 2b and 2d for a 90^{J} pulse inserted in the C(CO)NH pulse sequence (*18*) for isotopically labeled protein NMR, compared to normal results for the pulse sequence in Figs. 2a and 2c, respectively. In the middle of this method, polarization is transferred from $^{13}C\alpha$ nuclei to ^{13}CO (carbonyl) nuclei via the pulses

$$\cdots\text{–}\{90[C\alpha];\ 90[CO]\}\text{–}\eta\text{–}180[C\alpha]\text{–}(\theta-\eta)\text{–}\{180[CO];\ 180[N]\}\text{–}\theta\text{–}\cdots, \quad [K]$$

with the next step (not shown) being transfer of polarization to the ^{15}N nuclei of the peptide bonds. The antiphase spin state, $2CO_yC\alpha_z$, is refocused to CO_x during the 2η *J*-modulated period centered on the 180[Cα] pulse, where η is $(4J)^{-1}$ for the 55-Hz Cα-CO coupling. This occurs at the beginning of an overall 2θ delay centered on {180[CO]; 180[N]}, where θ is $(4J)^{-1}$ for the 15-Hz CO-N coupling, during which CO_x transforms to $2CO_yN_z$. If the 90[Cα] pulse is not applied, the spin state is $2CO_yC\alpha_x$ after 90[CO], and this can be transformed selectively to CO_x with a $90^{J_{CC}}$ pulse as in option [J] listed above for INEPT:

$$\cdots\text{–}\{90[CO];\ 90^{J_{CC}}[C\alpha]\}\text{–}(\theta-2\sqrt{2}\eta)\text{–}\{180[CO];\ 180[N]\}\text{–}\theta\text{–}\cdots, \quad [L]$$

where $2\sqrt{2}\eta$ is the length of the $90^{J_{CC}}$[Cα] pulse and 180[Cα] is no longer necessary.

Consequently, this method selects only those amino acids whose $^{13}C\alpha$ nuclei resonate within a bandwidth of approximately $J = 55$ Hz. A single slice at 46 ppm has been selected in Fig. 2b (the peaks at 27 and 31 ppm are side chain carbons correlated via the Cα nuclei at 46 ppm by a prior period of DIPSI-3 mixing). This slice is narrower than the strip of peaks in the normal spectrum (Fig. 2a), and three small peaks that coincide with the sinc wobbles are indicated in the expanded slice region above Fig. 2b. Of these, the larger negative wobbles may be suppressed by plotting positive contours only. Figure 2c shows the normal $^{15}N/^{1}H$ correlation contrasted with the selectivity obtained in Fig. 2d for the 90^{J} pulse. Very high selectivity is obtained without increasing the time length of the sequence. The overall pulse sequence structure is simplified by insertion of the 90^{J} pulse demonstrating that the new method is easy to apply.

This type of application, illustrated with the C(CO)NH sequence, will be useful whenever there is an advantage in converting a 3D method (^{13}C-^{15}N-^{1}H in this case) to a selective 2D correlation (^{15}N-^{1}H here). For example, repetitive measurements of dynamics such as relaxation times may be obtained on a set of selected resonances more quickly than by obtaining a complete 3D spectrum. The gains may be very large if these measurements are to be repeated as a function of pH, temperature, inhibitor concentration, etc. This is because selectivity in the 3D method is limited by the number of complex points, n_i, and the sweep width, SW, in the extra dimension. Resolution for a 90^{J} pulse may be defined as where the curve in Fig. 1b intersects zero signal amplitude at $\pm 0.8J = \pm 44$ Hz. For multidimensional NMR, resolution varies a little with the apodization method used, but the equivalent resolution is given approximately by $\pm SW/(2n_i)$. The minimum ^{13}C spectral width for aliphatic carbons (at 600 MHz for protons) is about 8800 Hz indicating that 100 complex points must be obtained to provide similar resolution to that shown in Figs. 2b and 2d. Since a minimum of two transients are required for each FID, and 200 FIDs are needed for the additional ^{13}C dimension, 400 transients must be acquired for each of 60 complex points in the ^{15}N dimension for the complete 3D spectrum. This compares to 64 transients for each of the 60 points to produce the spectrum in Fig. 2d. Accordingly, in this illustration a selective 2D spectrum can be obtained six times more quickly than a 3D spectrum with the same resolution.

This theoretical comparison between the selective 2D correlation and a full 3D method is confirmed by the spectra in Fig. 3. Two-dimensional slices are displayed in Figs. 3a and 3b obtained from 3D acquisitions with 32 and 100 complex points, respectively, in the carbon dimension. Within experimental error these 2D slices match the ^{13}C frequency of the $90^{J_{CC}}$[Cα] pulse in Figs. 2b and 2d. As expected, the Fig. 3a spectrum, which has low resolution in the ^{13}C dimension, contains several additional resonances to that in Fig. 2d. In contrast, the Fig. 3b slice is very similar to that of Fig. 2d. The ^{13}C resolution for Fig. 3b is probably still a little worse than that obtained with the 90^{J} pulse, but most of the minor differences are explicable in terms of a small ^{13}C frequency shift between the two spectra, which were obtained on different days.

There is also a gain in *S*/*N* ratio for the selective 2D example over the 3D method for the same acquisition time. For the ^{13}C dimension the 90° read pulse is either *x* or *y* phase for any single FID. That is, the quadrature detection of the ^{13}C frequency is not simultaneous so that on average *S*/*N* is reduced by $1/\sqrt{2}$ compared to the case of no ^{13}C chemical shift evolution. Accordingly, twice as many transients are required for the 3D method as for the selective 2D experiment to obtain the same *S*/*N*. An experimental comparison is shown in Fig. 4, where Fig. 4a is a trace at a ^{15}N shift of 128 ppm from Fig. 2d, and Fig. 4b is the equivalent trace from Fig. 3a. For the latter 3D experiment, twice as many transients were accumulated as for the 90^{J} spectrum, and the *S*/*N* ratios are equivalent as expected. This, however, is an oversimplification. There will be some loss of signal during the 90^{J} pulse because the Cα linewidths are a significant fraction of t_P^{-1}. But additional losses also occur for the 3D method, in particular from apodization of the t_1 FID, relaxation during the t_1 delay, homonuclear ^{13}C coupling, and t_1 noise. The comparison in Fig. 4 indicates that

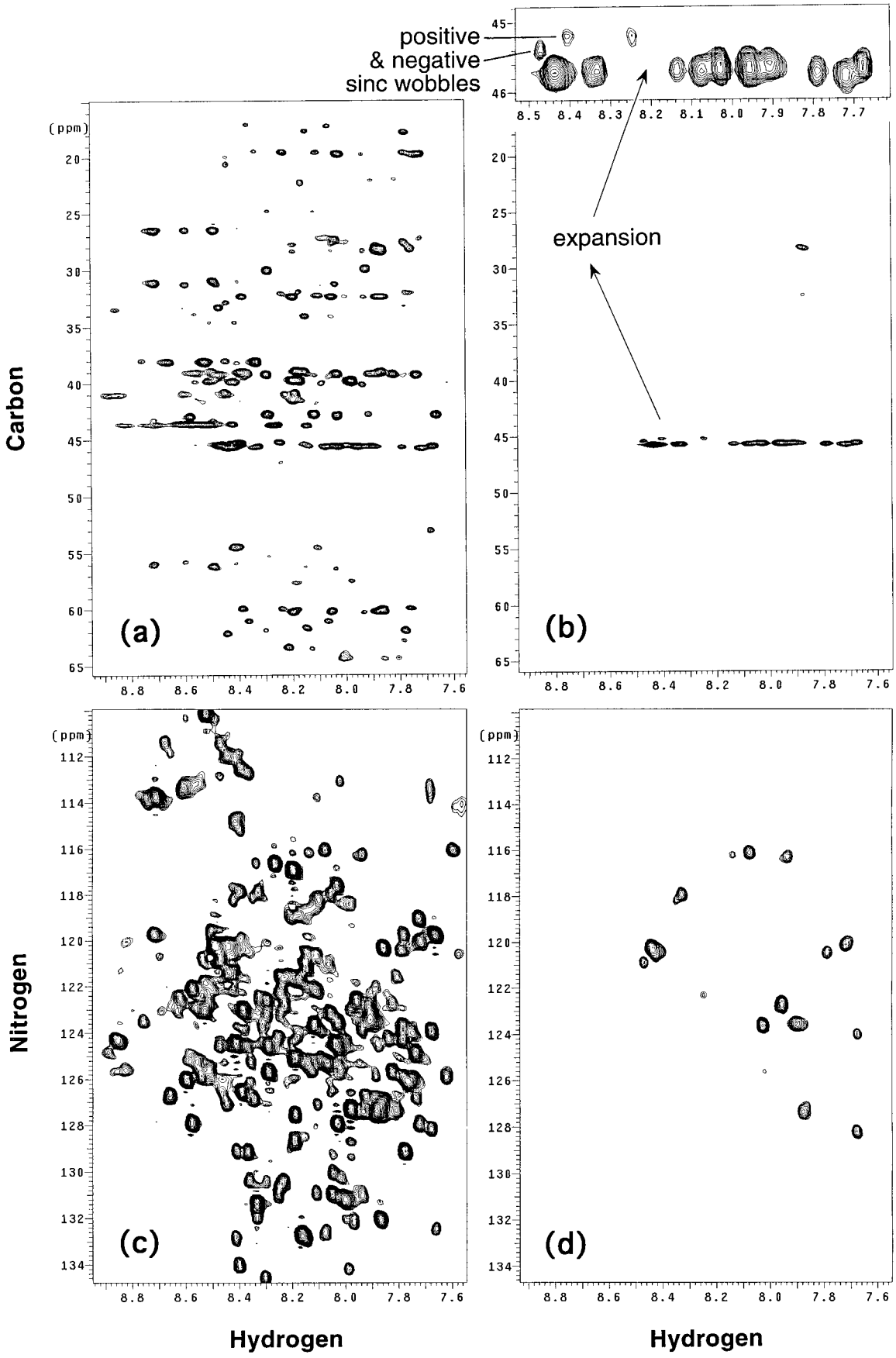
positive
& negative
sinc wobbles
expansion
Carbon
Nitrogen
Hydrogen
Hydrogen
(a)
(b)
(c)
(d)
(ppm)

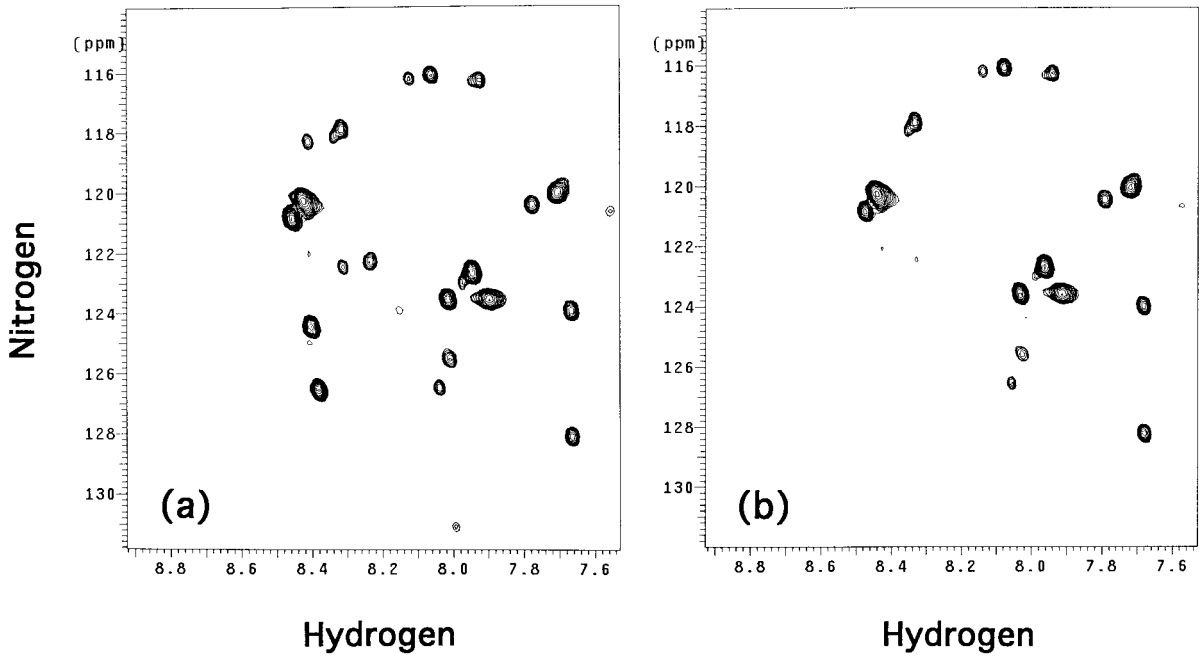

FIG. 3. Two-dimensional ^{15}NH–N^{1}H correlated planes of a 3D ^{13}Cα/β–^{15}NH–N^{1}H spectrum obtained using the C(CO)NH sequence as in Fig. 2. The planes correspond to the same ^{13}C frequency selected by the 90^{J} pulse in Figs. 2b and 2d. (a) 32 complex points were obtained for a ^{13}C spectral width of 8800 Hz—the spectrum shows poorer slectivity than that in Fig. 2d and needed twice as many transients. (b) As for (a) except that 100 complex points were acquired—the spectrum shows similar selectivity to that in Fig. 2d but required 6.25 times more transients.

these extra losses from the two different methods are similar and that the $1/\sqrt{2}$ loss for the 3D experiment dominates.

Thus there are gains in acquisition time for the same spectral resolution or the same S/N for this type of selective 90^{J} ^{13}C method compared to the equivalent multidimensional experiment. Of course, the selective method contains much less information in terms of correlated nuclei than the multidimensional technique, but a primary application as mentioned above will be in the repeated measurement of a few correlated resonances.

Another useful area of application is where a nonselective 3D pulse sequence can be converted into a selective 3D method. For example, the H(CCO)NH sequence (*18*) provides a C^{1}H′–^{15}NH–N^{1}H 3D correlation where ^{1}H′ nuclei are on the amino acid side chains. Since H(CCO)NH contains the same sequence elements [K] listed above, these can be converted to elements [L] ensuring that a C^{1}H′–^{15}NH–N^{1}H 3D correlation is obtained only for those amino acids selected by the $90^{J_{CC}}$[Cα] pulse. Thus, whenever crowding in the ^{1}H and ^{15}N spectra produces ambiguity for particular amino acids using a standard H(CCO)NH sequence, this can be easily overcome using the dispersion in the ^{13}C spectrum to select those particular residues without the need to obtain a time-consuming 4D spectrum. Another example from the same family is for the CbCa-(CO)NH sequence (*20*). The constant time (T_{AB}) ^{13}C chemical shift evolution period is long enough to allow replacement of the 90[H]–ϵ elements with 90^{J}[H] so that the original 3D method becomes a selective 3D technique with respect to a chosen aliphatic proton frequency.

Continuing with examples from the C(CO)NH sequence, any of the overall $(2J)^{-1}$ periods may be utilized for J pulses as described above for simple INEPT if the modest 40% increase in the length of these periods is acceptable. Pulses of the 180^{J} type may be used for the initial 90°–$(2J)^{-1}$ or $(2J)^{-1}$–90° periods as in schemes [E] and [F] and no refocusing pulses are needed because the RF is on resonance on the excited spins. However, as noted already, further work is needed to design shaped 180^{J} pulses so that their offset profiles are competitive with conventional counterparts of the same length. Any delay and an appropriate 90° pulse can also be replaced with 90^{J} as in schemes [G] and [J], but for a 90^{J}[I] pulse the 180[S] chemical-shift refocusing pulses at the center

FIG. 2. Two-dimensional spectra of ^{13}C/^{15}N isotopically enriched alphalytic protease obtained using the C(CO)NH pulse sequence (*18*) as implemented in (*19*). (a) Normal ^{13}Cα/β–N^{1}H correlation. (b) As for (a) but with a $90^{J_{CC}}$[Cα] pulse, B_1 = 28 Hz, length = 12.9 ms applied at 46 ppm in place of the normal 90[Cα]–η–180[Cα]–η–portion of the sequence. The slice selected at 46 ppm is expanded and displayed above (b). (c) Normal ^{15}NH–N^{1}H correlation. (d) As for (c) but with the $90^{J_{CC}}$[Cα] pulse substituted as in (b) to illustrate the selectivity obtained using the 90^{J} pulse. The peak at a ^{15}N shift of 127.4 ppm in (d) corresponds to the sidechain carbons at 27 and 31 ppm in (b) and is absent from Fig. 3 (see further details under Experimental).

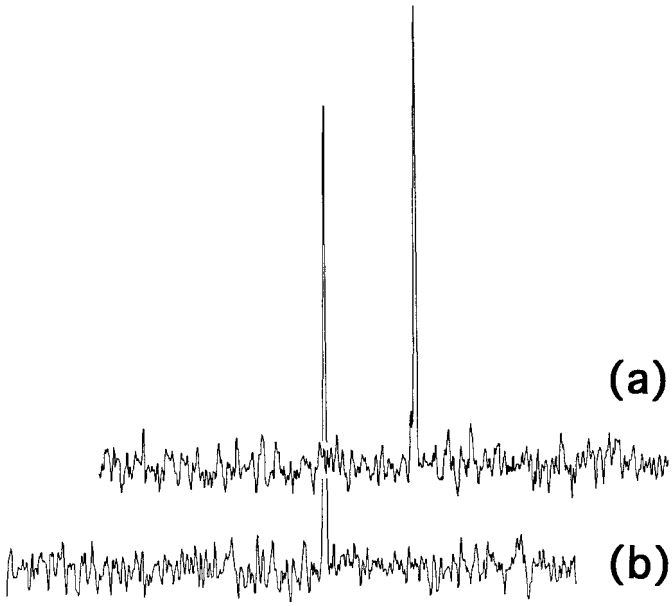

FIG. 4. ^{1}H spectra over a width of 6 ppm obtained at a ^{15}N shift of 128.2 ppm from (a) Fig. 2d and (b) Fig. 3a. The *S*/*N* ratios, defined as the signal height divided by the rms noise, are 19 and 20, respectively, but the second spectrum was obtained with twice as many transients as the first. The equivalent spectrum derived from Fig. 3b has a *S*/*N* ratio of 35 but was obtained with 6.25 times more transients than spectrum (a).

of the $(2J)^{-1}$ period must be retained. We find that whenever a 180[S] pulse occurs during a 90^{J}[I, *x*] pulse, the normal course of the *J* modulation operative during the *J* pulse on resonance is restored by applying a high-power "instantaneous" 180[I, *x*] inversion pulse simultaneously with 180[S]. Unfortunately this impairs the well-behaved offset profile as displayed in Fig. 1b so that it becomes similar to that of the 180^{J} pulse in Fig. 1a. Again improvements can be expected by shaping these 90^{J} pulses when they are overlapped by refocusing pulses, so that they can be applied optimally and generally.

COMPARISON WITH CONVENTIONAL METHODS

For a detailed comparison of *J* pulses with conventional selective-pulse methods, the offset profiles of one-lobe sinc 90° and 180° pulses, which have the same bandwidth at 0.5 signal amplitude as the 90^{J} pulse, are displayed in Figs. 1d and 1e, respectively. The 90^{J} pulse provides a bandwidth of *J* Hz (within 2%) at half height. The emphasis in this article is on importing frequency selectivity generally into pulse sequences with the minimum increase in their time length, and the one-lobe sinc (central lobe only, no side lobes) is optimally short for a conventional selective pulse (*19*). Indeed, the length of the sinc-90 pulse of Fig. 1d is $0.6J^{-1}$ s compared to $0.7J^{-1}$ s for the 90^{J} pulse of Fig. 1b. But as described for the C(CO)NH sequence, in favorable cases a 90^{J} pulse can be nested within a pulse sequence without increasing its length, and in the general case of substituting for an entire $(2J)^{-1}$ period it increases the time length by only $0.2J^{-1}$ s as already mentioned. In contrast, the entire length of the conventional selective pulse is additional to a sequence. Moreover, conventional methods cannot be applied to pulse sequences by simply substituting a soft pulse for a hard pulse, because the spins are modulated by scalar coupling during the long soft pulse in ways that only now can be fully described (*4*). Any attempt to take this modulation into account leads full circle back to *J* pulses. If a soft pulse is substituted for a hard excitation pulse acting on in-phase S-spin magnetization, the I spins must be decoupled (*13*). If the substitution is for a hard 90° pulse in an INEPT transfer step, or for the equivalent step in HMQC, the transverse coupled spins must be uncoupled by spin locking during the selective pulse (*21*) and *S*/*N* loss may occur if the spin locking does not adequately cover the full spectral width.

Furthermore, it is clear from the comparison of Figs. 1d and 1b that the shaped sinc-90 pulse provides a worse profile than the 90^{J} pulse even though the latter is rectangular. Better conventional pulses than the sinc can be employed but any improvement in the profile comes at the expense of a longer pulse. For example, a half-Gaussian shape does not induce negative signal lobes, but to produce a bandwidth of *J* Hz at half height its length is $0.9J^{-1}$ s (*22*). However, it is not possible to devise a reasonable conventional experiment that is equivalent to scheme [L] even if the time penalty of $0.9J^{-1}$ s for a half-Gaussian is accepted. The prime difficulty is as follows. To prevent coupling effects during a soft 90[Cα] conventional pulse in scheme [K], the 90[CO] pulse could be applied first and the resulting transverse ^{13}CO spins might be uncoupled by spin locking during the soft pulse. But the coupled spins are homonuclear and it would be difficult to retain the integrity of the soft pulse at one frequency while spin locking at another.

The more common type of conventional selective pulse is the soft inversion pulse. Scalar coupling effects are refocused during all symmetric inversion pulses so no decoupling or spin locking of the nonirradiated spin is necessary. It is well known that shaped inversion pulses provide much better offset profiles than the equivalent 90° pulses, and this is illustrated in Fig. 1e for a conventional sinc-180 pulse. But, unsurprisingly, the sinc-180 is twice as long at $1.2J^{-1}$ s. Except in special cases such as the heteronuclear spin-echo difference experiment (*23*), the use of inversion pulses to import selectivity into pulse sequences requires additional pulse sequence segments containing the soft pulse. In the case of methods such as spin-pinging (*24*) and DANTE-Z (*25*) these additional segments are optimally equal to the length of the soft pulse, but other techniques such as excitation sculpting (*26*) require extra pulsed-field-gradient delays and even repetition of the soft pulse. In all cases the extra time requirement is greater than J^{-1} s.

In applications as in Fig. 2 it will generally be acceptable to suppress moderate negative contours by not plotting them, and

so the offset profile for the 90^J pulse in Fig. 1b is a little better than that for sinc-180 in Fig. 1e. If this is not acceptable then the 90^J profile is a little worse than sinc-180 profile. Overall we can say that the two pulses are competitive in terms of frequency selectivity. Unlike the sinc-90 case, a selective inversion method can be readily added to scheme [K]. For example, a sinc-180 pulse could be inserted between the 90[Cα] and 90[CO] pulses in [K] when the spin state is $2CO_zC\alpha_z$. If inserted for alternate transients as in the DANTE-Z technique with alternate subtraction of signal (*25*), a similar result to scheme [L] will be achieved. This method will not be as stable as scheme [L] because it relies on the cancellation of unwanted signal outside the selected bandwidth by addition/subtraction, whereas in scheme [L] using *J* pulses the nonselected spins remain unobservable in the $2CO_yC\alpha_x$ state. But if a time penalty of $1.2J^{-1}$ s for the sinc-180 is acceptable then why not double it and use the more stable excitation sculpting method? If that is acceptable then the sinc-180 pulses should be replaced with much longer pulses with rectangular offset profiles such as BURP pulses (*25*). Thus, solely in terms of ideality of frequency profiles, it will always be possible to implement a conventional method that is better than a rectangular 90^J pulse.

This, however, is a complete departure from the basic premise of this article. Our thesis is that if the most important performance criterion is the length of the pulse sequence, as it will be for large molecules, then there are no conventional methods that are competitive with *J* pulses.

There is one 90° pulse, the Janus pulse (*27*), that might be termed conventional in that it does not make use of *J* modulation, but still induces the spin state transformation, $S_z \rightarrow 2S_yI_z$ and so could take the place of a $90°–(2J)^{-1}$ combination at the beginning of a pulse sequence. However, the Janus pulse was designed for a different purpose to be effective over a factor of 10 variation in coupling constant, so it has a length of about $5J^{-1}$ s relative to average *J*. There is no indication in Ref. (*27*) that this pulse could be redesigned for a single *J* to be competitive with the 180^J pulse of Brondeau and Canet (*12*).

CONCLUSIONS

A new class of frequency-selective RF pulses has been demonstrated. These utilize *J* modulation during the irradiation to selectively transform a weakly coupled IS-spin system between in-phase magnetization and a two-spin product operator state. Potentially, these *J* pulses are generally applicable in pulse sequences since they can replace any combination of a hard 90° pulse and a $(2J)^{-1}$ free-precession period as in the pulse sequence elements, $90°–(2J)^{-1}$ or $(2J)^{-1}–90°$. Unlike conventional selective pulses, *J* pulses minimally increase the time length of pulse sequences and so have advantages in systems subject to rapid relaxation. Like conventional selective pulses, there are gains in reducing the acquisition times for multidimensional methods, especially for repetitive measurements using the same pulse sequence and sample.

In the specific applications described here, a 90^J pulse was implemented in its simplest form as a rectangular pulse, and it was shown to be competitive with the shortest of amplitude-modulated pulses on the basis of off-resonance selectivity. A further advantage in terms of limiting the time length of a pulse sequence was gained by entirely nesting the pulse within the parent sequence and, although demonstrated for a particular group of sequences, this type of application should find use throughout the class of triple-resonance sequences employed for biomolecular NMR. Because *J* pulses are selective, they can be used as easily in homonuclear methods as heteronuclear sequences (the Fig. 2 illustration is a homonuclear example).

Furthermore, we suggest that the three main limitations of the present illustration of *J* pulses may be lifted in the future:

- Rectangular 180^J pulses, and rectangular 90^J pulses that are overlapped by refocusing pulses, are not competitive with conventional methods in terms of offset profiles. These profiles should improve with the substitution of pulse shapes designed via numerical simulations in an analogous way to their conventional counterparts.[1]
- *J* pulses uniformly operate on the whole multiplet, yet, as currently implemented, they have an impressive minimum bandwidth of *J* Hz. Nevertheless this is restrictive and many applications require greater spectral widths. It should be possible to reduce the extent of *J* modulation during the pulse and so provide any bandwidth.
- The analytical equations for any I_mS or IS_n group (*4*) will determine the conditions for selective *J* pulses on systems with more than two coupled nuclei.

Removal of these limitations would realize the potential general applicability of the *J* pulse method at which time a convenience factor should become apparent—any high-resolution pulse sequence can be made selective with respect to any group of weakly coupled spins by one simple change.

EXPERIMENTAL

The experimental points in Fig. 1c were obtained using a standard HCN triple-resonance PFG probe on a 500-MHz Varian INOVA spectrometer using a 2% sample of the isopropyl ester of $^1H^{13}CO_2H$ in $CDCl_3$, doped with 0.2% $Cr(AcAc)_3$ relaxation agent. The B_1 calibration method that was employed is described in more detail in Ref. (*15*). Briefly, signifying $S \equiv {}^1H$ and $I \equiv {}^{13}C$, CW decoupling of the I spins during signal detection of the S spins yields a centerband with amplitude $1 - (J/2B_e^J)^2$, and sidebands at

[1] *Note added in proof.* Except for overlapping refocusing pulses, these problems have been solved as described in the subsequent comprehensive paper referred to in the body of the text and now submitted for publication.

$\pm B_e^J$ with amplitude $0.5(J/2B_e^J)^2$, where $B_e^J = [B_1^2 + (J/2)^2]^{0.5}$. B_1 was calibrated to within 1 dB of $J/2$ Hz (111 Hz) from the difference in frequency between these sidebands, which is $\sqrt{2}J$ when $B_1 = J/2$. Values of signal magnitude as a function of resonance offset for the $S_x \rightarrow 2S_yI_y$ transformation were obtained by measuring antiphase $2S_yI_z$ signal at $\pm J/2$ Hz with sequence [M],

$$90[\mathrm{S}, -y]; 90^J[\mathrm{I}, x]; 90[\mathrm{I}, \pm x]; \text{acquire S}[\pm]. \quad [\mathrm{M}]$$

The final pulse in [M] converts $2S_yI_y$ to $2S_yI_z$.

The spectra in Fig. 2 were obtained using a standard HCN triple-resonance PFG probe on a 600-MHz Varian INOVA spectrometer using a sample of doubly labeled alphalytic protease. The C(CO)NH pulse sequence (*18*) with minor modifications as implemented in Ref. (*19*) was used for Figs. 2a and 2c. For Figs. 2b and 2d scheme [L] was employed. The phase shift, induced on the homonuclear ^{13}CO spins by the $^{13}C\alpha$ pulses (*18*), was calibrated by adjusting the phase of the subsequent 90[CO] pulse to null the 1D signal, and 90° was then added to this phase to eliminate the shift. This adjustment changes when the 90^J pulse is substituted as in scheme [L]. For Figs. 2a and 2b, 64 transients were acquired for each of 128 complex points in t_1 with the ^{13}C spectral width set at 10,300 Hz. For Figs. 2c and 2d, 64 transients were obtained for 60 complex points in t_2 for a ^{15}N width of 2200 Hz. The ^{13}C width was reduced to 8800 Hz and 2 transients were acquired for 60 complex points in t_2, and 32 and 100 complex points in t_1 for Figs. 3a and 3b, respectively. For the Fig. 3 spectra, a cosine-squared apodization window was applied whose time length exceeded the number of acquired points in t_1 by 25% to maximize resolution and S/N by permitting small sinc wobbles on either side of resonances—these wobbles are not displayed in Fig. 3. The apodization functions used in Figs. 2 and 3 for the ^{1}H and ^{15}N dimensions were the same for all spectra. Most of the $^{13}C\alpha$ resonances selected in Fig. 2b are from glycine residues. However, the side chain signals at 27 and 31 ppm in Fig. 2b, which correlate with the peak at 127.4 ppm in Fig. 2d, are detected via a $^{13}C\alpha$ nucleus that resonates at 46 ppm but which produces no C(CO)NH signal and is therefore absent from Fig. 3. $^{13}C\alpha^1$H moieties do not necessarily provide a correlation using the C(CO)NH sequence as demonstrated by strip plot 6, Fig. 2a, Ref. (*18*).

REFERENCES

1. M. R. Bendall, *J. Magn. Reson. A* **116,** 46 (1995).
2. T. E. Skinner and M. R. Bendall, *J. Magn. Reson.* **134,** 315 (1998).
3. M. R. Bendall and T. E. Skinner, *J. Magn. Reson.* **129,** 30 (1997).
4. T. E. Skinner and M. R. Bendall, *J. Magn. Reson.* **141,** 271–285 (1999).
5. J. S. Waugh, *J. Magn. Reson.* **49,** 517 (1982).
6. A. J. Shaka and J. Keeler, *Prog. NMR Spectrosc.* **19,** 47 (1987).
7. W. A. Anderson and R. Freeman, *J. Chem. Phys.* **37,** 85 (1962).
8. C. Griesinger, O. W. Sorensen, and R. R. Ernst, *J. Magn. Reson.* **73,** 574 (1987).
9. C. Zwahlen, P. Legault, S. J. F. Vincent, J. Greenblatt, R. Konrat, and L. E. Lewis, *J. Am. Chem. Soc.* **119,** 6711 (1997).
10. E. Kupce and R. Freeman, *J. Magn. Reson.* **127,** 36 (1997).
11. A. A. Chalmers, K. G. R. Pachler, and P. L. Wessels, *J. Magn. Reson.* **15,** 415 (1974); H. J. Jakobsen, P. J. Kanyha, and W. S. Brey, *J. Magn. Reson.* **54,** 134 (1983); and references contained therein.
12. J. Brondeau and D. Canet, *J. Magn. Reson.* **47,** 419 (1982).
13. G. A. Morris and R. Freeman, *J. Magn. Reson.* **29,** 433 (1978).
14. R. Bazzo and J. Boyd, *J. Magn. Reson.* **79,** 568 (1988).
15. M. R. Bendall and T. E. Skinner, *J. Magn. Reson.* **139,** 175 (1999).
16. G. A. Morris and R. Freeman, *J. Am. Chem. Soc.* **101,** 760 (1979).
17. M. R. Bendall, D. T. Pegg, and D. M. Doddrell, *J. Magn. Reson.* **45,** 8 (1981).
18. S. Grzesiek, J. Anglister, and A. Bax, *J. Magn. Reson. B* **101,** 114 (1993).
19. M. R. Bendall, *in* "ProteinPack" (M. R. Bendall, G. Gray, and B. John, Eds.), Varian, Palo Alto (1997).
20. S. Grzesiek and A. Bax, *J. Am. Chem. Soc.* **114,** 6291 (1992).
21. J.-M. Bernassau and J.-M. Nuzillard, *J. Magn. Reson. A* **104,** 212 (1993).
22. J. Friedrich, S. Davies, and R. Freeman, *J. Magn. Reson.* **75,** 390 (1987).
23. M. R. Bendall, D. T. Pegg, D. M. Doddrell, and J. Field, *J. Am. Chem. Soc.* **103,** 934 (1981).
24. P. Xu, X. L. Wu, and R. Freeman, *J. Magn. Reson.* **99,** 308 (1992).
25. C. Roumestand, J. Mispelter, C. Austruy, and D. Canet, *J. Magn. Reson. B* **109,** 153 (1995).
26. T. Hwang and A. J. Shaka, *J. Magn. Reson. A* **112,** 275 (1995).
27. E. Kupce and R. Freeman, *J. Magn. Reson. A* **104,** 234 (1993).